

## Electron-hopping modes in $\text{NiMn}_2\text{O}_{4+\delta}$ materials

R. Schmidt,<sup>a)</sup> A. Basu, and A. W. Brinkman

University of Durham, Department of Physics, South Road, Durham DH1 3LE, United Kingdom

Z. Klusek and P. K. Datta

University of Northumbria, Advanced Materials Research Institute, Newcastle upon Tyne NE1 8ST, United Kingdom

(Received 28 May 2004; accepted 12 January 2005; published online 7 February 2005)

The resistance versus temperature ( $R$ - $T$ ) characteristics of  $\text{NiMn}_2\text{O}_{4+\delta}$  thermistors have been analyzed. In the literature, electron transport in manganate spinels is commonly described by a small-polaron model for nearest neighbor hopping, but variable range hopping (VRH) has not been considered so far. In this study differentiated  $R$ - $T$  data were analyzed, allowing a clear distinction between different modes of hopping. In pressed pellets and thick screen printed films conduction was well described by a VRH model for a parabolic density of states, which was confirmed by scanning tunneling spectroscopy. © 2005 American Institute of Physics. [DOI: 10.1063/1.1866643]

In  $\text{NiMn}_2\text{O}_{4+\delta}$  electron transport is thought to be accomplished by small polaron hopping between  $\text{Mn}^{3+}$  and  $\text{Mn}^{4+}$  cations,<sup>1,2</sup> where the mixed valence of manganese arises because the spinel is not regular but partially inverted. A fraction  $x$  of the  $\text{Ni}^{2+}$  cations are displaced from tetrahedral to octahedral interstices of the oxygen fcc sublattice, a corresponding proportion  $2x$  of  $\text{Mn}^{3+}$  cations on octahedral sites disproportionate to  $\text{Mn}^{2+}$  and  $\text{Mn}^{4+}$ , and the  $\text{Mn}^{2+}$  cations move to the tetrahedral sites to compensate  $\text{Ni}^{2+}$  vacancies.<sup>3</sup> Electrical conductivity in  $\text{NiMn}_2\text{O}_{4+\delta}$  is sensitive to the concentration of donor ( $\text{Mn}^{3+}$ ) and acceptor ( $\text{Mn}^{4+}$ ) electron states and therefore also to the inversion parameter  $x$ , which in turn is dependent on the sintering history of the sample. Sintering history also affects the oxygen stoichiometry  $\delta$ , which again changes the  $\text{Mn}^{3+}/\text{Mn}^{4+}$  ratio.<sup>2</sup> Such sensitivity to sample history has led to a great variety of resistance versus temperature ( $R$ - $T$ ) characteristics and an equally diverse set of models,<sup>4,5</sup> including some that are purely empirical.

The Jahn-Teller distortion of the  $\text{Mn}^{3+}$  cations leads to the formation of polarons, whereby electrons are thought to be localized (small polarons) due to the strong ionic character of the bonding in spinel crystals. The strong electron-phonon coupling results in highly temperature dependent phonon assisted  $\text{Mn}^{3+}/\text{Mn}^{4+}$  small polaron hopping, which also occurs in CMR manganite perovskites although in that case supported by double exchange interactions mediated by the oxygen anions.<sup>1</sup> This does not occur in the spinel manganates and conduction may be understood from a simple real space picture of localized electrons bound to  $\text{Mn}^{3+}$  states, in contrast to conventional semiconductors where delocalized electrons are described in momentum space.<sup>6</sup> Macroscopically,  $\text{Mn}^{3+}/\text{Mn}^{4+}$  hopping of strongly localized electrons is a percolation problem with a percolation threshold parameter  $\xi_C$  that includes both spatial and energy contributions<sup>7</sup>

$$\xi_C \geq \frac{2r_{ij}}{a} + \frac{\varepsilon_{ij}}{k_B T}, \quad (1)$$

where  $r_{ij}$  and  $\varepsilon_{ij}$  are the separation in real and energy space of the  $i$  and  $j$  electron states respectively,  $k_B$  is the Boltzmann constant, and  $a$  is a localization length that scales the acceptor and donor wave functions. The relative magnitudes of the two terms on the right-hand side of Eq. (1) determine whether or not hopping is constrained to nearest neighbors, and evidently at sufficiently high temperatures it always is. A general expression for the resistivity  $\rho$  for all type of hopping transport can be formulated  $\{\rho = \rho_0 \exp(\xi_C)\}$ , where  $\rho_0$  and  $\xi_C$  depend on particular physical and material properties of the system. This can be elaborated for polaron nearest neighbor hopping (NNH) and variable range hopping (VRH) models, which leads to the generalized expression for both cases

$$\rho(T) = CT^\alpha \exp\left(\frac{T_0}{T}\right)^p, \quad (2)$$

where  $C$  is a constant. In the case of NNH,  $\alpha = p = 1$  and the characteristic temperature  $T_0$  is proportional to  $\varepsilon_{ij}$  only, as  $r_{ij}$  is constant. For VRH  $\alpha = 2p$  and together with  $T_0$  depends principally on the shape of the density of states (DOS).<sup>8</sup> For a uniform DOS (i.e., Mott hopping)  $p = \frac{1}{4}$ , for a parabolic distribution of the DOS around the Fermi level  $p = \frac{1}{2}$ .

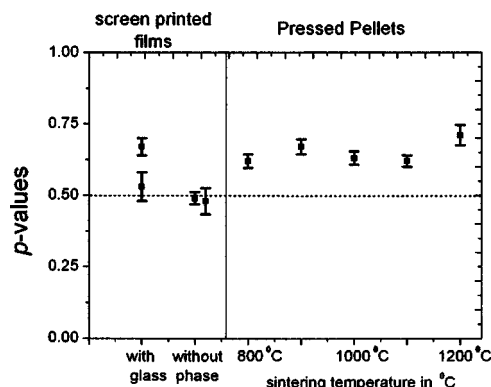


FIG. 1. Summary diagram of  $p$  values for screen-printed films with and without an added glass phase and pressed pellets sintered at different temperatures.

<sup>a)</sup> Author to whom correspondence should be addressed; present address: University of Cambridge, Department of Materials Science and Metallurgy, Pembroke Street, Cambridge CB2 3QZ, United Kingdom; electronic mail rs441@cam.ac.uk

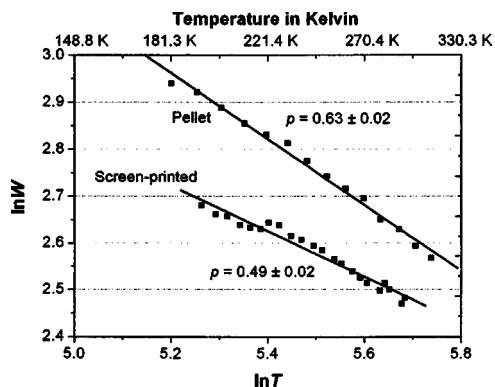


FIG. 2. Representative  $\ln(W)$  vs  $\ln(T)$  plots for a pressed pellet and a screen-printed film. For clarity, the pellet graph has been displaced up the  $\ln(W)$  axis by 0.1 units.

The (dc)  $R$ - $T$  characteristics for pressed pellets and thick screen printed films were compared by analysis of the index parameter  $p$ . Data were taken in the range of 150–500 K using Al contacts, which were evaporated on the samples surface and were covered with a silver layer to prevent oxidation. The data were analyzed following a procedure described by Shklovskii and Efros,<sup>8</sup> where it is possible to determine  $p$  from the slope of a plot of  $\ln(W)$  vs  $\ln(T)$ :

$$W = \frac{1}{T} \frac{d(\ln \rho)}{d(T^{-1})} \approx -p \left( \frac{T_0}{T} \right)^p. \quad (3)$$

This is a powerful technique to elucidate the character of hopping motion, but it is a differentiation method and is therefore sensitive to scatter in the original  $R$ - $T$  data.

Source powder from a conventional precursor oxide method was pressed into pellets; starting material used for screen printing was prepared by coprecipitation of precursor mixed oxalates and their subsequent firing. Thick films (25–30  $\mu\text{m}$ ) were printed onto  $\text{Al}_2\text{O}_3$  substrates; one type of

film included an additional glass phase, another set of samples was printed without glass. Sample preparation methods and structural characterization are described elsewhere.<sup>9,10</sup> Results from the differential analysis of the  $R$ - $T$  data are summarized in Fig. 1 and representative  $\ln(W)$  vs  $\ln(T)$  plots for each type of sample are shown in Fig. 2. In thick screen-printed films  $p$  values were close to 0.5, implying that conduction was by VRH with a parabolic DOS. Similar, though slightly higher  $p$  values were found for the pressed pellets. Figure 3 shows representative  $R$ - $T$  data of a pellet sintered at 800 °C and a screen-printed film including a glass phase, plotted on two different axes.

(1) The  $\ln(\rho)$  vs  $1/T$  curves are bended uniformly for both types of sample as confirmed by the good linearity of the differentiated data graphs in Fig. 2. A linear fit was performed to determine the average characteristic temperature  $T_0$  as shown in Fig. 3, but these values were corrected by taking into account that the pre-exponential factor is temperature dependent according to Eq. (2). Plotting  $\ln(\rho/T)$  vs  $1/T$  gave 3233 K for the pellet and 3454 K for the film, the activation energies ( $E_A = k_B T_0$ ) were 0.28 and 0.30 eV respectively.

(2) The data were much better described by a plot of  $\ln(\rho/T)$  vs  $1/T^{0.5}$  appropriate for VRH with a parabolic shape of the DOS. By assuming a DOS of the form  $g(\epsilon) = g_0 \cdot \epsilon^2$ , and using the  $\text{Mn}^{3+}/\text{Mn}^{4+}$  cation radii from a hard sphere model as an upper limit for  $a$ ,<sup>11</sup> a lower limit for  $g_0$  can be obtained from  $T_0$  according to Mansfield.<sup>7</sup> But evidence from impedance spectroscopy<sup>12</sup> suggested that  $a \approx 0.3 \text{ \AA}$  and an estimated value for  $g_0$  was obtained. The values of  $g_0$ , the resistivity  $\rho_{RT}$  at 20 °C and  $T_0$  for pellets and films are summarized in Table I.

$P$  values below 1 indicate a change of activation energy with temperature, but only if the hopping distance  $r$  changes as well the situation can be described as VRH. In conventional semiconductors  $p$  values  $< 1$  can be associated with a

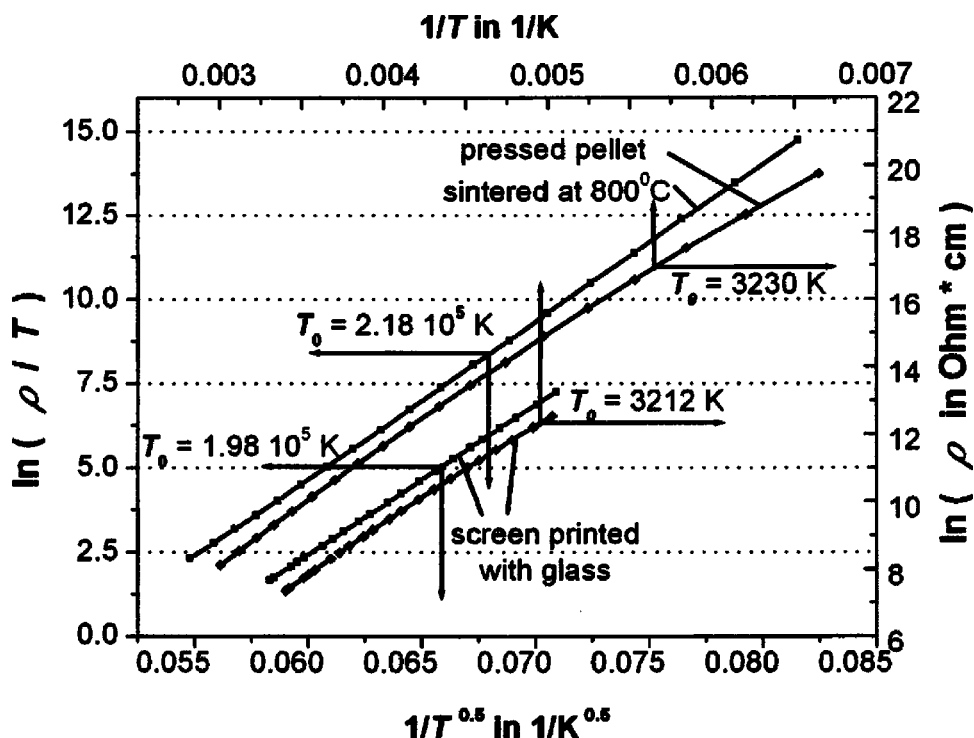


FIG. 3. Plot of  $\ln(\text{resistivity})$  vs  $1/T$  and  $\ln(\text{resistivity}/T)$  vs  $1/T^{0.5}$ .

TABLE I.  $T_0$ ,  $\rho$ , and  $g_0$  for pellets sintered at different temperatures and films printed with and without glass.

	Pressed pellets					Printed films	
	800 °C	900 °C	1000 °C	1100 °C	1200 °C	With	Without
$T_0/\text{K}$	$2.18 \times 10^5$	$2.25 \times 10^5$	$2.28 \times 10^5$	$2.28 \times 10^5$	$2.20 \times 10^5$	$1.98 \times 10^5$	$2.10 \times 10^5$
$\rho/\Omega \text{ cm}$	$1.5 \times 10^4$	$1.5 \times 10^4$	$7.0 \times 10^3$	$6.63 \times 10^3$	$3.7 \times 10^3$	$1.6 \times 10^3$	$0.86 \times 10^3$
$g_0$ in $\text{eV}^{-3} \text{ cm}^{-3}$	$3.5 \times 10^{23}$	$3.2 \times 10^{23}$	$3.1 \times 10^{23}$	$3.1 \times 10^{23}$	$3.4 \times 10^{23}$	$4.7 \times 10^{23}$	$4.0 \times 10^{23}$

sole change in activation energy, if localized electrons in the band gap are activated from charge carrier traps or donor states of varying energy into the delocalized conduction band. This is not a valid approach in  $\text{NiMn}_2\text{O}_{4+\delta}$ , where electrons are always strongly localized due to the ionic type of crystal bonding, and the variations in activation energy lead to a change in the maximum hopping distance as well, and to VRH. The parabolic shape of the DOS in  $\text{NiMn}_2\text{O}_{4+\delta}$  may arise from electron–electron interactions, but nonuniform crystal strain due to inhomogeneous electron-phonon interactions or grain boundary effects may lead to deviations from a strict parabolic relationship and explain the deviations of  $\rho$  in the pellets.

In order to investigate the energy distribution of the DOS in  $\text{NiMn}_2\text{O}_{4+\delta}$ , STS measurements were carried out on thin ( $\sim 200$  nm) films, sputter deposited on  $\langle 100 \rangle$  oriented Si substrates. Sample preparation methods and the STS apparatus setup are described in detail elsewhere.<sup>13,14</sup> It had been shown there that the shape of the DOS is parabolic with a broad gap, but here more detailed low energy STS results are shown in Fig. 4 as a plot of the DOS versus electron energy. It is suggested that the shape of the DOS may be consistent

with Hubbard type bands below and above the Fermi level at  $\sim 0.1$  eV within the broad gap, corresponding to  $\text{Mn}^{3+}$  and  $\text{Mn}^{4+}$  cations, respectively. The  $g(\epsilon)$  values determined from  $g_0$  (Table I) at 0.1 eV are in the order of  $\sim 4 \times 10^{21} \text{ eV}^{-1}/\text{cm}^{-3}$ , which is two orders of magnitude lower than for crystalline Ge at the conduction band edge. The Hubbard bands evolve more clearly at higher temperatures, which it is believed to be an artifact of the measurement. The  $\text{Mn}^{3+}/\text{Mn}^{4+}$  charge transfer rate rather than the gap between sample and tip may be limiting the tunneling current at lower temperatures as the films exhibited a high dc resistance of  $\sim 10^8 \Omega$  at room temperature.

In conclusion, VRH associated with a parabolic DOS appears to be the dominant electron transport process. STS suggested that the parabolic shape may arise from Hubbard type bands.

A.B. acknowledges financial support from the Overseas Research Scholarship (ORS) scheme and the University of Durham.

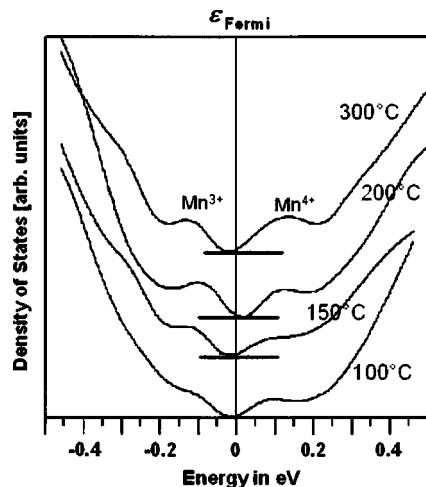


FIG. 4. Low energy STS, DOS vs electron energy at different temperatures; the DOS at Fermi level was always zero.

<sup>1</sup>N. Tsuda, K. Nasu, A. Fujimori, and K. Siratori, in *Electronic Conduction in Oxides*, Solid-State Sciences, edited by M. Cardona *et al.* (Springer, Berlin, 2002).

<sup>2</sup>E. D. Macklen, *Thermistors* (Electrochemical Publications, Glasgow, 1979).

<sup>3</sup>V. A. M. Brabers and J. C. J. M. Terhell, *Phys. Status Solidi A* **69**, 325 (1982).

<sup>4</sup>J. A. Becker, C. B. Green, and G. L. Pearson, *Bell Syst. Tech. J.* **26**, 170 (1947).

<sup>5</sup>A. Feltz, J. Töpfer, and F. Schirmeister, *J. Eur. Ceram. Soc.* **9**, 187 (1992).

<sup>6</sup>G. Kotliar and D. Vollhardt, *Phys. Today* **57**(3), 53 (2004).

<sup>7</sup>R. Mansfield, in *Hopping Transport in Solids*, edited by M. Pollak and B. Shklovskii (Elsevier Science, Amsterdam, 1991).

<sup>8</sup>B. I. Shklovskii and A. L. Efros, *Electronic Properties of Doped Semiconductors*, Solid State Sciences 45 (Springer, Berlin, 1984).

<sup>9</sup>R. Schmidt, A. Stiegelschmitt, A. Roosen, and A. W. Brinkman, *J. Eur. Ceram. Soc.* **23**, 1549 (2003).

<sup>10</sup>R. Schmidt, A. Basu, and A. W. Brinkman, *J. Eur. Ceram. Soc.* **24**, 1233 (2004).

<sup>11</sup>A. Navrotsky and O. J. Kleppa, *J. Inorg. Nucl. Chem.* **29**, 2701 (1967).

<sup>12</sup>R. Schmidt, Ph.D. thesis, University of Durham, 2003.

<sup>13</sup>A. Basu, Ph.D. thesis, University of Durham, 2002.

<sup>14</sup>A. Basu, A. W. Brinkman, Z. Klusek, P. K. Datta, and P. Kowalczyk, *J. Appl. Phys.* **92**, 4123 (2002).